*Desalination and Water Treatment*
www.deswater.com
doi: 10.5004/dwt.2021.27496

231 (2021) 425–435
August

# Solid state dispersion and hydrothermal synthesis, characterization and evaluations of $TiO_2$/ZnO nanostructures for degradation of Rhodamine B

Siamak Dolatabadi[a], Moslem Fattahi[a,*], Mohammad Nabati[b]

[a]*Department of Chemical Engineering, Abadan Faculty of Petroleum Engineering, Petroleum University of Technology, Abadan, Iran, email: fattahi@put.ac.ir (M. Fattahi), siamak1917@gmail.com (S. Dolatabadi)*
[b]*Department of Basic Sciences, Abadan Faculty of Petroleum Engineering, Petroleum University of Technology, Abadan, Iran, email: nabati@put.ac.ir*

Received 4 January 2021; Accepted 1 June 2021

**ABSTRACT**

In this study, $TiO_2$/ZnO nanostructures were synthesized by sol–gel solid-state dispersion method and hydrothermal methods for degradation of Rhodamine B (RhB). The ZnO weight percentage, calcination temperature and irradiation time were investigated for synthesizing the different catalyst samples. Then, the X-ray diffraction, Brunauer–Emmett–Teller, Fourier-transform infrared spectroscopy and field emission scanning electron microscopy analysis was performed to characterize the as-prepared catalysts. The experimental design was utilized for photocatalytic degradation of RhB. The effects of operating parameters such as pH, irradiation time, initial RhB concentration and catalyst concentration were investigated through this study. The degradation tests were performed by UV of 24 W. The best degradation performance of 99.28% was obtained. The results of characterization and degradation via two methods of preparation including the; sol–gel and hydrothermal were analyzed and compared. Besides, the optimum conditions for reaching the highest RhB degradation were reported.

*Keywords:* Hydrothermal; Sol–gel; Photocatalyst degradation; Rhodamine B; Experimental design; Solid-state dispersion

## 1. Introduction

Rhodamine B (RhB) is one of the dyes used in the textile, cosmetics, biotechnology laboratories and etc. It has a highly complex organic compound and because of the complexity of its structure, it can be a good benchmark for experiments. Advanced oxidation process (AOP) type procedures can become very promising technologies for treating wastewater containing non-biodegradable or hardly biodegradable organic compounds with high toxicity [1].

Amongst AOPs methods photocatalytic degradation has proven to be a promising technology for degrading refractory organic matters. Metal oxide semiconductors such as $TiO_2$, ZnO, MgO, $ZrO_2$ have been attempted for the photocatalytic degradation of a wide variety of environmental contaminants [2,3]. $TiO_2$ as a catalyst has several advantages but for more activation, ultraviolet (UV) will be used and for better efficiency using another catalyst such as ZnO besides $TiO_2$ will be appropriate. It can reduce electron–hole recombination and cause increased efficiency.

An ideal photocatalyst for photocatalytic oxidation is characterized by the following attributes including photostability, chemically and biologically inert nature, availability and low cost. $TiO_2$ is the most preferred one due to its chemical and biological inertness, high photocatalytic activity, photo-durability, mechanical robustness and cheapness.

* Corresponding author.

The titanium photocatalytic efficiency might be enhanced by metals and non-metals doping. Therefore, combining $TiO_2$ with other suitable semiconductors such as ZnO, $Fe_3O_4$, CuO, MgO can be reduced electron–hole recombination of photo-electrons and improved efficiency [4–9].

Although numerous researches on the removal of different organic pollutants from wastewater using $TiO_2$/ZnO as photocatalyst nanocomposite has already been performed, however, the interfacial ZnO charge transfer rate is low and both of the aforementioned photocatalysts alone have a large bandgap and high electron-hole recombination rate. Furthermore, both of them have a great tendency to aggregation, especially at high concentrations. Hence, to enhance the photocatalytic activity and to solve the aggregation problem, the addition of different compounds such as various biopolymers and carbon materials to the semiconductors as solid supports is a suitable approach [10–12]. Recycling and separation of photocatalysts are considerable problems in the practical approach. Solid supports played a significant role in facilitating catalyst's immobilization [11]. It was also reported that supported materials can increase the surface area of catalytic systems and thus improve in hydrophobicity, thermal, hydrolytic, and chemical stability of the catalysts occurred [13].

Pei et al. [14] studied $TiO_2$/ZnO nanofibers that have been synthesized with a small diameter having 10 nm poly-crystallites of large surface area by electrospinning followed by calcination. The photocatalytic activities of nanofibers have been studied systematically by the degradation of RhB dye under the 420 nm visible-light irradiation (degradation is 90%). Chen et al. [15] investigated novel titanium dioxide ($TiO_2$) and zinc oxide (ZnO) hybrid photocatalysts in the form of nanofibers that have been fabricated by a facile method using electro-spinning followed by a calcination process. The photocatalytic performances have been evaluated via the photo-degradation of RhB under irradiation with UV light (degradation is 90%). Zha et al. [16] have used nanostructured $TiO_2$/ZnO heterojunctions with the morphologies of hedgehogs and fan blades have been synthesized by a solvothermal method (97% MO degradation under UV light within 30 min). Pozan and Kambur [17] studied ZnO-$TiO_2$ binary oxide catalysts that have been successfully prepared by a solid-state dispersion. Xu et al. [18] focused on the composite powder of $TiO_2$/ZnO with an atomic ratio of Ti to Zn of 3/1 has been prepared through sol–gel process followed by hydrothermal and post-heat treatments.

Zhuge et al. [19] showed that $Ti_3C_2T_x$ promoted the photocatalytic efficiency of pure $CaIn_2S_4$ for degradation of different hazardous contaminants. Besides, the hybrid of $CaIn_2S_4$-$Ti_3C_2T_x$ showed a higher photocurrent density than pure $CaIn_2S_4$. Liu et al. [20] showed that the catalysts of $Cu_2In_2ZnS_5$ and $Gd_2O_2S$:Tb by providing more active sites improved the photocatalytic reduction activity for Cr(VI) and $CO_2$. Liu et al. [21] showed photocatalytic and photoelectrochemical activity of pure $ZnIn_2S_4$ by UiO-66 addition attributed more active sites for pollute adsorption. Based upon band-edge levels constructed in the ZU hybrids, the UiO-66 could enhance the separation of photo-induced charge carriers and prolong their lifetime. Ren et al. [22] showed $MoSe_2$/ZnO/ZnSe hybrids improved photocatalytic reduction ability under visible light irradiation compared to pure ZnO. The introduction of $WS_2$ as a co-catalyst can prolong the charge carrier lifetime that enhancing the catalytic activity of $CaIn_2S_4$ for efficient Cr(VI) reduction [23].

In the current study, sol–gel via solid-state dispersion (SSD) method and hydrothermal for the synthesis of $TiO_2$/ZnO nanostructures were utilized. The efficiency of synthesized nano $TiO_2$/ZnO investigated for degradation of RhB. The characteristics of the synthesized nano $TiO_2$/ZnO determined by X-ray diffraction (XRD), field emission scanning electron microscopy (FESEM), Brunauer–Emmett–Teller (BET) and Fourier-transform infrared spectroscopy (FTIR). The efficiency of these two methods of synthesis was compared. Moreover, the operating parameters of pH, irradiation time, initial RhB concentration as well as catalyst dosage were studied through this study.

## 2. Experimental

### 2.1. Materials

Titanium tetrachloride ($TiCl_4$) and zinc nitrate hexahydrate $Zn(NO_3)_2{\cdot}6H_2O$ from Merck Company, (Germany) was purchased and utilized as the titanium and zinc precursors. Besides, ethanol (Merck Company, Germany) and deionized water as the solvent and $NH_4OH$ as the pH adjuster was utilized.

### 2.2. Catalyst preparation

#### 2.2.1. Sol–gel and SSD synthesis of nano $TiO_2$/ZnO

Pristine $TiO_2$ was prepared through sol–gel method. 8 mL $TiCl_4$ was slowly added dropwise into 80 mL ethanol solution at room temperature (sol of $TiO_2$) in which a large amount of HCl gas was exhausted during the mixing process. Then, a light yellow solution was obtained and gelatinized for 5 h at 80°C in the oven to form sol–gel and for aging, it remained at room temperature for 40 h. Finally, the gel was dried in the oven at 110°C for 12 h, ground into a fine powder, and calcined at 500°C for 2 h. In addition, the ZnO was prepared by the co-precipitation technique. 25 g of zinc nitrate hexahydrate was dissolved in 100 mL deionized hot water and the resulting solution was heated up to 65°C. This mixture was precipitated by gradually adding $NH_4OH$ solution (6 mol $L^{-1}$) until the pH value reached 10. The resultant solution was slowly stirred for 2 h at 65°C (sol of ZnO). The precipitate was then filtered, washed with deionized water and dried at 100°C for 16 h and then calcined at 500°C for 5 h.

Since the time of gelatinization of two catalysts not equal, ZnO-$TiO_2$ binary oxide catalysts were prepared by the SSD method. SSD method initially involves mixing $TiO_2$ and ZnO thoroughly using ethanol. The solvent was then removed by evaporation while mixing. Samples prepared by this method were dried at 110°C and calcined at 350°C, 550°C and 750°C for 6 h to obtain ZnO-$TiO_2$ binary oxide catalysts. ZnO amount of the catalysts was nominally 20 and 33 wt% and reported as the weight percentage. The different conditions of prepared catalysts through SSD method was provided in Table 1. For instance, 1:4 ZnO-$TiO_2$ and 1:2 ZnO-$TiO_2$ mean that the catalyst contained nominally 20% and 33% ZnO by weight [17,24].

*2.2.2. Hydrothermal synthesis of nano $TiO_2$/ZnO*

The prepared ZnO sol was then directly incorporated into the $TiO_2$ sol at an atomic molar ratio of Zn to Ti of 1:4 and 1:2 to achieve the ZnO/$TiO_2$ composite sol. The mixture of $TiO_2$/ZnO sol was aged for a period of time at room temperature until it became gel. The gel was dried and pulverized to be powder. The gel powder was then transferred into a Teflon-lined autoclave and heated at various temperatures for different times (200°C and 150°C for 12 and 24 h). After hydrothermal treatment, the powder was washed with distilled water and dried. The powder was finally post-heat treated by calcination in the air for 8 h at 550°C in a muffle oven [18]. The condition of synthesized catalysts through hydrothermal method was summarized in Table 2.

*2.3. Characterization*

The crystal structure and phase of nanomaterials were characterized by XRD (Model: Philips, PW 1730 diffractometer, Netherlands) using Cu $K_\alpha$ radiation ($\lambda$ = 0.15,406 nm) by scanning in angular range (2θ) from 10° to 80°. The particle size and morphology of $TiO_2$/ZnO were studied with scanning electron microscopy (FESEM-TESCAN MIRA3, Kohoutovice, Czech Republic) which was equipped with energy-dispersive X-ray spectroscopy (EDXS). FTIR spectra were recorded between the wavenumber of 400 and 4,000 $cm^{-1}$ (Bruker, Model: VERTEX 70, Germany). The specific surface area (BET method), specific pore volume and average pore diameter (Barrett, Joyner, Halenda method) were determined by using nitrogen adsorption at 77 K (Model: BELSORP MINI 3, Czech Republic).

*2.4. Experimental design*

Response surface methodology (RSM) is a powerful mathematical and statistical design tool that can be used to evaluate and optimize the performance of complex systems by considering the relative significance of several affecting factors even in the presence of complicated, multi-dimensional interactions [2]. To investigate the effect of operating parameters including the; pH, time, initial RhB concentration and catalyst concentration, Design-Experts software (Ver. 7.0.0) was employed for the design of experiments and mathematical modeling.

The effect of pH in the range of 3, 6 and 9; time in the range of 3, 4 and 5 h; initial RhB concentration in the range of 1, 2 and 3 mg $L^{-1}$ and catalyst concentration in the range of 0.2, 0.3 and 0.4 g $L^{-1}$ were investigated.

Table 1
The prepared catalysts via the SSD method in this research

| Catalyst sample | Weight percentage of ZnO (%) | Calcination temperature and time (*T*, °C/time, h) |
|---|---|---|
| S1 | 20 | 350/6 |
| S2 | 20 | 550/6 |
| S3 | 20 | 750/6 |
| S4 | 33 | 350/6 |
| S5 | 33 | 550/6 |
| S6 | 33 | 750/6 |

*2.5. Photocatalytic activity tests*

The photocatalytic activity of nano $TiO_2$/ZnO with different operational parameters for degradation of RhB in aqueous solution was carried out using a setup that consists of a cylindrical quartz reactor (for better UV transmission) with magnetic stirring and six 4W-UVC lamps that covered it also an opaque plastic cover was placed outside to isolate other light sources. The pH value of the solution was adjusted by adding a small amount of 0.1 M NaOH or HCl and monitoring with a digital pH meter. For each test, various amount of catalyst was added into a quartz-reactor containing 30 mL of the RhB with defined concentration. The mixture was stirred for 10 min in the dark to adsorption and desorption equilibrium. After desired time samples were centrifuged for 15 min at a rate of 12,000 rpm to separate photocatalysts and obtain a transparent solution. The final concentration of RhB was determined by a UV-vis spectrophotometer at $\lambda_{max}$ = 554 nm.

Finally, for calculation of the degradation rate of RhB the following equation was used:

$$\text{Degradation}\,(\%) = \frac{C_0 - C_t}{C_0} \times 100 \quad (1)$$

where $C_0$ is the initial concentration of RhB (mg $L^{-1}$) and $C_t$ is the final concentration of RhB (mg $L^{-1}$) after degradation time.

## 3. Results and discussion

*3.1. XRD analysis*

XRD analysis in Fig. 1 indicates the formation of the pure anatase phase of $TiO_2$ and zincite phase of ZnO in all samples S1, S2 and S5 that synthesized by sol–gel method

Table 2
The prepared catalysts via hydrothermal method in this investigation

| Catalyst sample | Weight percentage of ZnO (%) | Hydrothermal temperature and time (°C/h) | Calcination temperature and time (°C/h) |
|---|---|---|---|
| H1 | 20 | 200/12 | 550/8 |
| H2 | 20 | 150/24 | 550/8 |
| H3 | 33 | 200/12 | 550/8 |
| H4 | 33 | 150/24 | 550/8 |

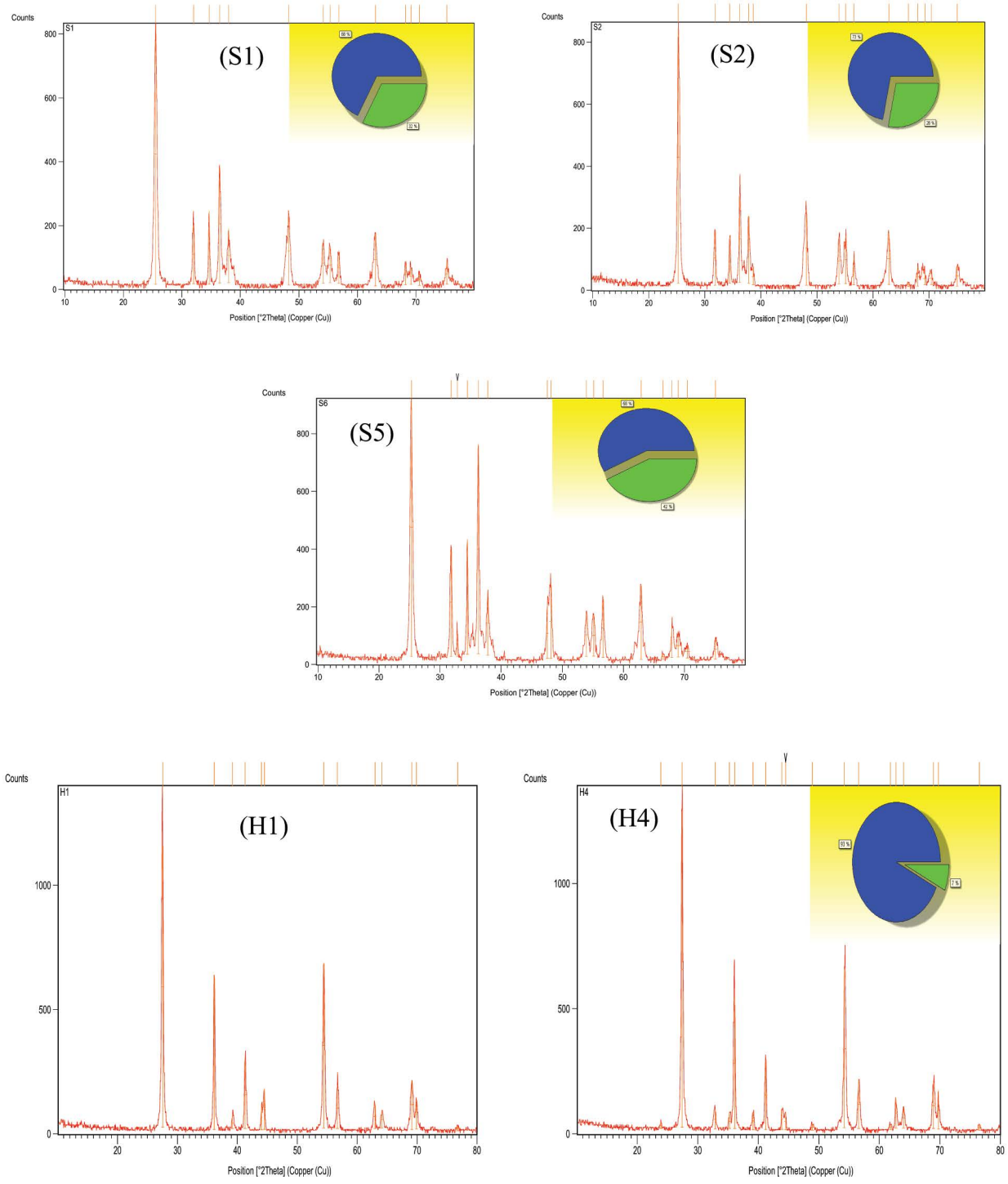


Fig. 1. XRD analysis pattern of the synthesized materials by sol–gel and hydrothermal methods in this research.

and the formation of pure rutile phase of $TiO_2$ and zincite phase of ZnO in both samples H1 and H4. The average size of $TiO_2$/ZnO crystallites was estimated by means of the Debye–Scherrer's equation on the main peak:

$$D = \frac{K\lambda}{\beta\cos\theta} \quad (2)$$

where $D$ is the average crystallite size, $K$ the constant which is taken as 0.89 here, $\lambda$ = 0.15406 nm is the wavelength of the X-ray radiation, $\beta$ is full width at half-maximum (FWHM), and $\theta$ is the diffraction angle [25]. The crystallite sizes, for samples S1, S2 and S5 are 19.17 nm, 16.77 nm and 14.90 nm, and for samples, H1 and H4 are 26.94 nm and 11.18 nm. It seems that in sol–gel method by increasing

the calcination temperature, the size of particles has been reduced but in a hydrothermal method the calcination temperature is the same, by increasing the hydrothermal time and hydrothermal temperature reduction, the size of particles has been reduced.

### 3.2. BET analysis

The surface area, pore-volume, and pore diameter of samples were measured using the $N_2$ adsorption method [3]. The surface area, total pore volume and mean pore diameter of samples are shown in Table 3.

As will be seen in FESEM analysis, it seems that by increasing the calcination temperature, aggregation of particles has been occurred and caused a reduction in surface area and total pore volume for sample S6 than sample S2. Moreover, the weight (%) of ZnO in sample S6 is more than S2 that might be effective in this reduction. Besides, the calcination temperature of samples H2 and H3 is the same, the total pore volume of the two samples is very near together but the difference in hydrothermal temperature and time caused the surface area of sample H2 to be greater than H3 probably.

The $N_2$ adsorption–desorption isotherms for sample S2 fitted type IV isotherms, for sample S6 fitted type III isotherm, and for samples, H2 and H3 fitted type V isotherm according to the IUPAC nomenclature is presented in Fig. 2. Adsorption on mesoporous solids proceeds via multilayer adsorption followed by capillary condensation, resulting in Type IV isotherm. Characteristic features of the type IV isotherm are its hysteresis loop, which is associated with capillary condensation taking place in mesopores, and the limiting uptake over a range of high $P/P_0$. This isotherm is used for porous materials and often be seen for industrial catalysts. Its hysteresis indicates mesopores structure's existence in the material. The reversible type III isotherm indicates an unrestricted multilayer formation

Table 3
The surface area, total pore volume and mean pore diameter of prepared samples

| Sample | Surface area ($m^2\ g^{-1}$) | Total pore volume ($cm^3\ g^{-1}$) | Mean pore diameter (nm) |
|---|---|---|---|
| S2 | 36.138 | 0.1602 | 17.732 |
| S6 | 6.4853 | 0.0207 | 12.793 |
| H2 | 39.514 | 0.3771 | 38.173 |
| H3 | 25.957 | 0.3916 | 60.364 |

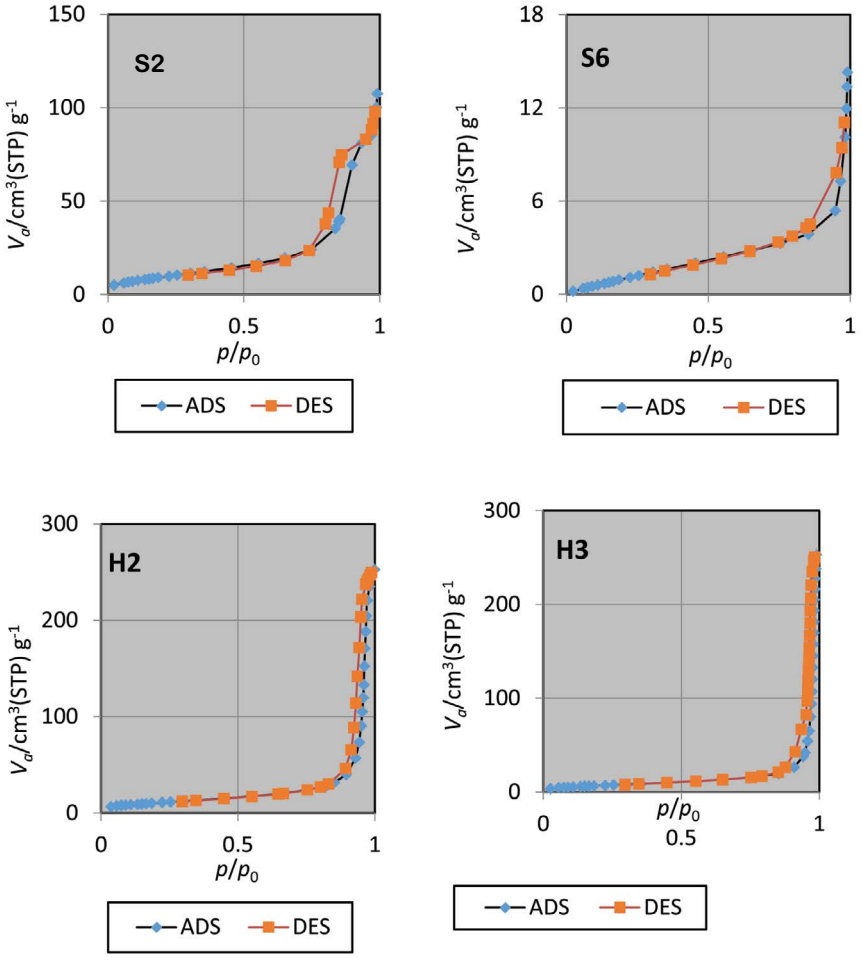


Fig. 2. $N_2$ adsorption/desorption isotherm of samples S2, S6, H2 and H3.

process. It forms because lateral interactions between adsorbed molecules are strong in comparison to interactions between the adsorbent surface and adsorbate. Nonporous systems have this isotherm. Type V isotherm is very similar to type III and is seen in porous materials including mesopores [26]. The $N_2$ adsorption–desorption isotherms for all samples are shown in the following Fig. 2:

To determination of pore size distributions, the Barrett, Joyner, Halenda (BJH) method was used. The classification of pore sizes: micropores (<2 nm) mesopores (2~50 nm) macropores (>50 nm) [26]. According to BJH plots in Fig. 3, all samples are mesopores but in sample S6 some pore sizes are micro and in sample H3 some pore sizes are macro.

### 3.3. FTIR analysis

FTIR spectroscopy can identify the positions at which the functional groups are attached. The reason is that vibrational frequencies differ when functional groups are attached at different sides in molecules [2]. FTIR analysis for all samples is shown in Fig. 4.

Several peaks related to $TiO_2$ are observed in all samples. The broadband centered at 500–600 $cm^{-1}$ is likely due to the vibration of the Ti–O bonds in the $TiO_2$ lattice [27]. For all samples in the study, two strong absorption bands were observed at ~430 and ~520 $cm^{-1}$. While the band at ~430 $cm^{-1}$ corresponds to the $E_2$ model of hexagonal ZnO, the band at ~520 $cm^{-1}$ may be associated with oxygen deficiency and/or oxygen vacancy (VO) defect complex in ZnO [28]. Also the peak at ~1,634.00 $cm^{-1}$ is corresponds to Zn–O stretching and deformation vibration [29]. In all samples, the 1,600 $cm^{-1}$ assigned to the hydroxyl groups and the ~600 $cm^{-1}$ band was associated with the Ti–O–Ti stretching vibration [30–35].

### 3.4. FESEM analysis

In order to investigate the surface morphology of the materials, samples S1, S2, S4, S6 and samples H1, H2 and H3 were analyzed by FESEM. The results are shown in Fig. 5.

Fig. 5 shows that synthesized samples by the hydrothermal method are more uniform than samples prepared by sol–gel method. Moreover, synthesized samples by the hydrothermal method are rod-like in shape. Sample S4 is mainly a sphere-like shape and sample S6 is not uniform and not a sphere or rod-like shape. The crystal size distribution is from 13.51 to 27.69 nm which is not very different from the XRD calculated sizes. Calcination temperature in sample S2 is greater than S1 that caused more aggregation of particles also great calcination temperature in sample S6 caused complete aggregation and as was seen in BET analysis, the surface area and total pore volume of sample S6 are very low. In samples H1, H2 and H3 that their calcination temperature and time are the same, aggregation of particles are similar but an aggregation of particles in sample H1 is less than H2 and H3. Less aggregation caused more surface area and more total pore volume.

The PL and UV-Vis absorption spectrum analysis for $TiO_2$/ZnO has been done by Zhang et al. [4].

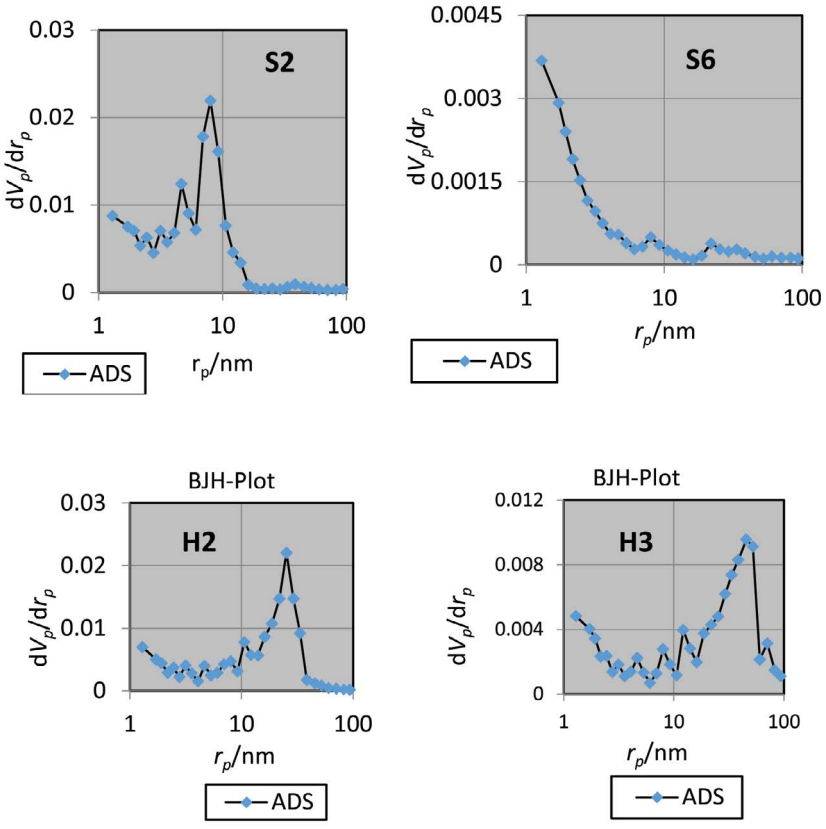


Fig. 3. BJH plots of samples S2, S6, H2 and H3.

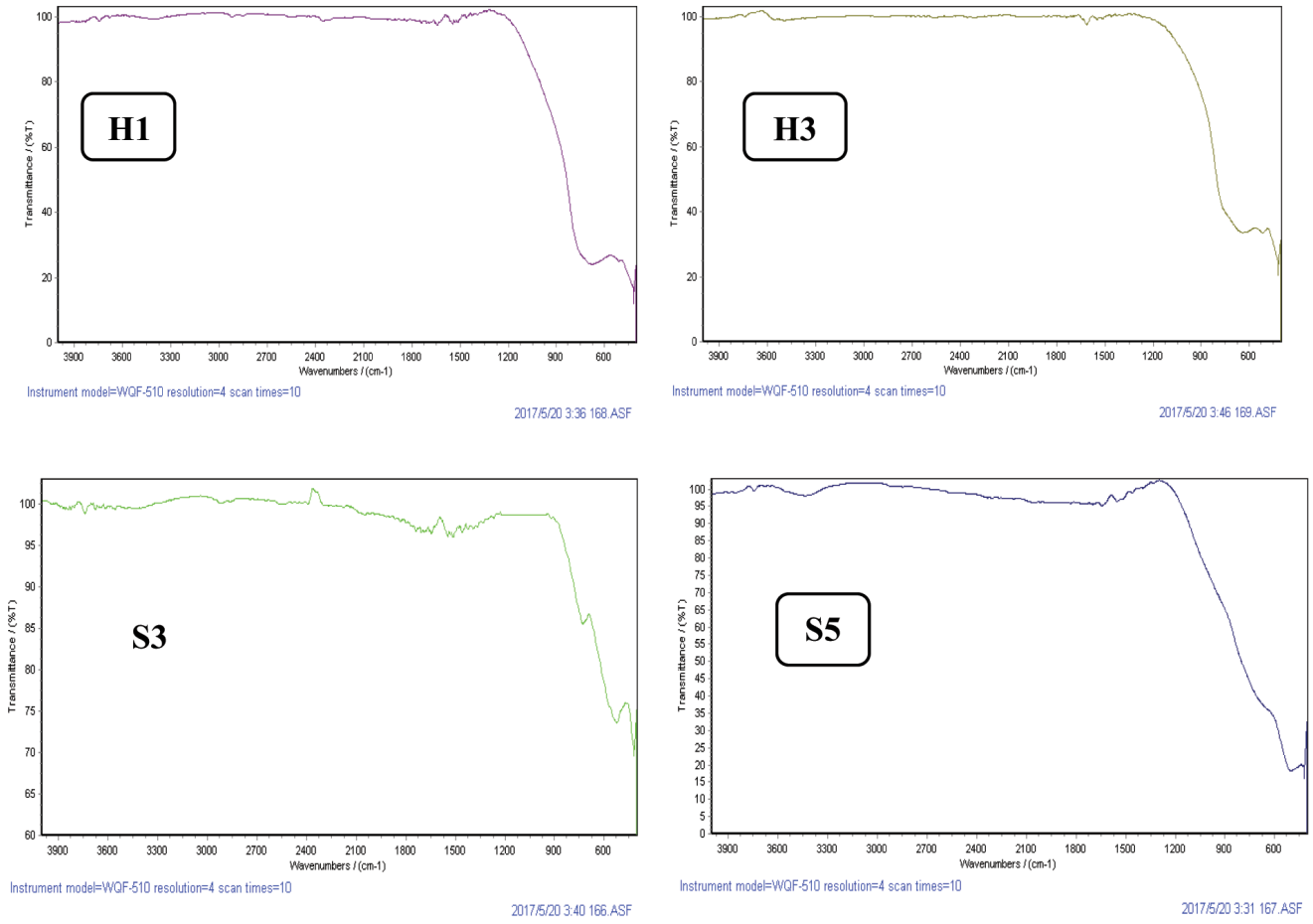


Fig. 4. FTIR spectra of the prepared catalysts in this investigation.

Their results showed that the composite materials reduce the recombination probability. The unique heterostructure photocatalyst of $TiO_2$/ZnO has a positive effect on the effective separation of photogenerated carriers during the photocatalytic reactions charge carriers. The visible light absorption intensity of $TiO_2$/ZnO improved compared in compare to ZnO or $TiO_2$. Moreover, according to the valence band position of $TiO_2$ and conduction band position of ZnO, $TiO_2$/ZnO nanocomposite is formed typical Type-II [4].

### 3.5. Experimental results

The photocatalytic powers of all samples for RhB degradation were compared together under the same conditions. The photocatalytic tests were performed at the conditions including; pH = 6, time = 4 h, initial concentration of RhB = 2 mg $L^{-1}$, catalyst concentration = 0.2 g $L^{-1}$, solution volume of 30 mL and power of UV 24 W (all mixture was stirred for 10 min in the dark to reach the adsorption–desorption equilibrium) in Figs. 6 and 7 to select the suitable catalyst.

Sample S1 (96.43% degradation) and H1 (92.39% degradation) were selected for photocatalytic degradation tests of RhB. To investigate the effects of operational parameters on RhB degradation, experiments were performed by Design-Expert® 7.0.0 software for samples S1 and H1. The best degradation of RhB by sample S1 was 99.28% and by sample, H1 was 98.57% (time: 5 h, initial RhB concentration: 2 mg $L^{-1}$, catalyst dosage: 0.3 g $L^{-1}$).

### 3.6. Optimum conditions

Optimum conditions for sample S1, to maximize the degradation of RhB by maximum initial RhB concentration and minimum concentration of catalysts were obtained at this conditions: pH = 5.54, time = 5 h, initial RhB concentration = 3 mg $L^{-1}$, Catalyst dosage = 0.2 g $L^{-1}$. Degradation at these optimum conditions correlated 94.98% compared with the experimental result of 95.75% which illustrated the good accuracy.

Besides, for sample H1, optimum conditions in maximum degradation of RhB by maximum initial RhB concentration and minimum concentration of catalyst were obtained at the conditions: pH = 5.74, time = 5 h, initial RhB concentration = 3 mg $L^{-1}$, Catalyst concentration = 0.2 g $L^{-1}$. Degradation at these optimum conditions correlated 91.96% compared with the experimental result of 92.91% which illustrated the good accuracy.

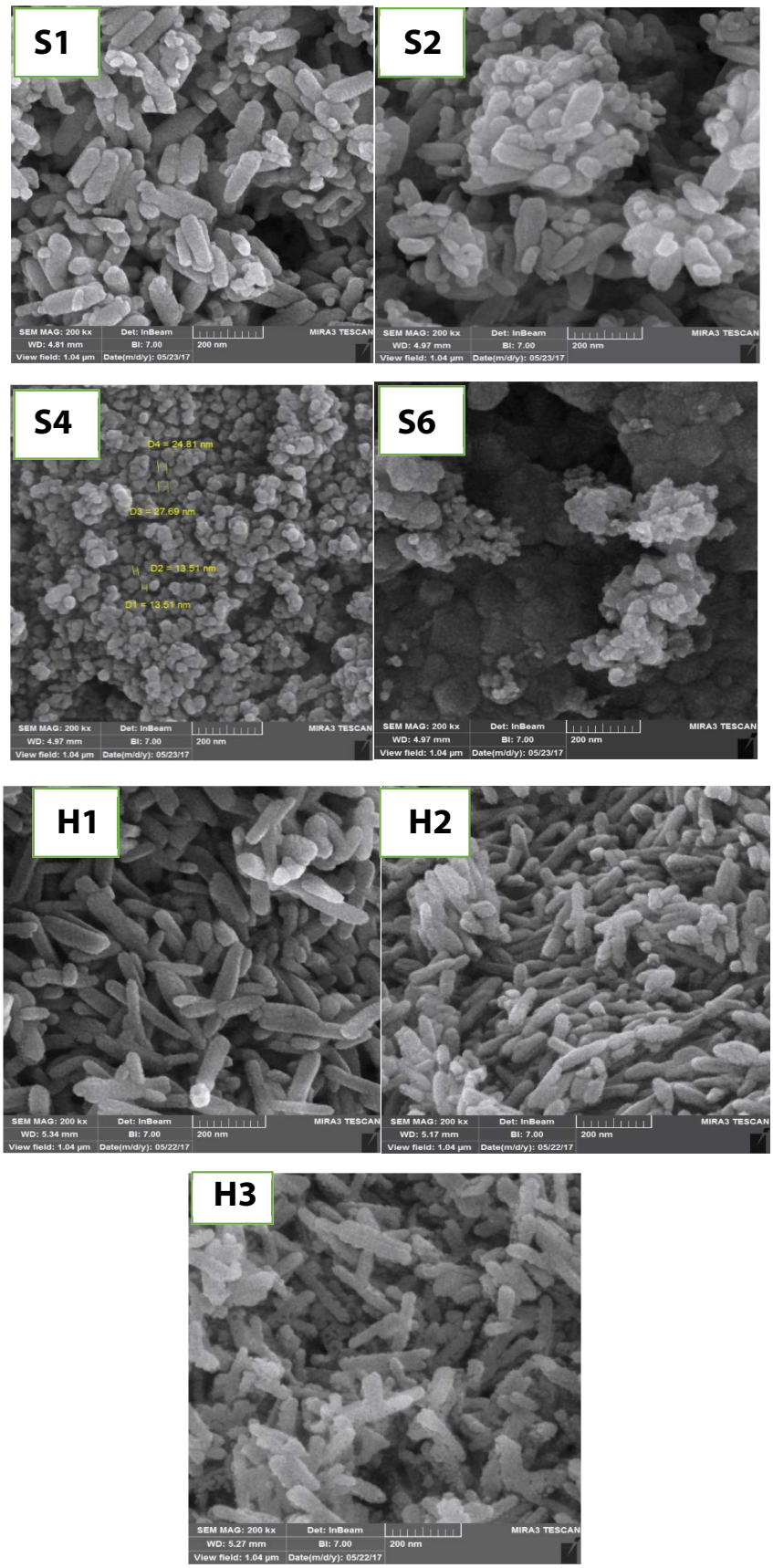


Fig. 5. FESEM analysis of synthesized samples.

### 3.7. Mechanism

Based on researches in the open literature [10,36] regarding photocatalysis a probable mechanism and photodegradation reactions of organic RhB using $TiO_2$-ZnO oxide materials as proposed below:

$$TiO_2/ZnO\ photocatalysts + hv \rightarrow e^- + h^+ \quad (3)$$

$$h^+ + H_2O \rightarrow H^+ + OH^\bullet \quad (4)$$

$$h^+ + OH^- \rightarrow OH^\bullet \quad (5)$$

$$h^+ + Rhodamine\ B \rightarrow oxidation\ products \quad (6)$$

$$e^- + O_2 \rightarrow {}^\bullet O_2 \quad (7)$$

$${}^\bullet O_2^- + 2H^+ \rightarrow H_2O_2 \quad (8)$$

$$e^- + H_2O_2 \rightarrow OH^\bullet + OH^- \quad (9)$$

$$e^- + Rhodamine\ B \rightarrow reduction\ products \quad (10)$$

$$Rhodamine\ B + OH^\bullet + O_2 \rightarrow CO_2 + H_2O + other\ decomposition\ products \quad (11)$$

## 4. Conclusions

$TiO_2$/ZnO nanostructures were synthesized by sol–gel (sol–gel and SSD) and hydrothermal methods in various wt%, calcination temperatures, hydrothermal temperatures and hydrothermal times. XRD, BET, FTIR, and FESEM analyses were performed to characterize the catalysts. Combining $TiO_2$ with other suitable semiconductors such as ZnO might be reduced electron–hole recombination of photo-electrons and improved efficiency. All samples synthesized by sol–gel method have an anatase phase, however, samples synthesized by the hydrothermal method have a rutile phase. Synthesized samples by the hydrothermal method are more uniform than synthesizes samples by sol–gel method. Moreover, synthesized samples by the hydrothermal method are more rod-like in shape. The total pore volume and surface area of samples prepared by the hydrothermal method are larger than sol–gel method.

The results of degradation tests for all samples have been reported, from these results, it will be concluded that samples prepared by the hydrothermal method are better for degradation of RhB, although the best degradation has been obtained by sample S1 that synthesized by sol–gel method. The best degradation of RhB by sample S1 was 99.28% and by sample, H1 was 98.57%.

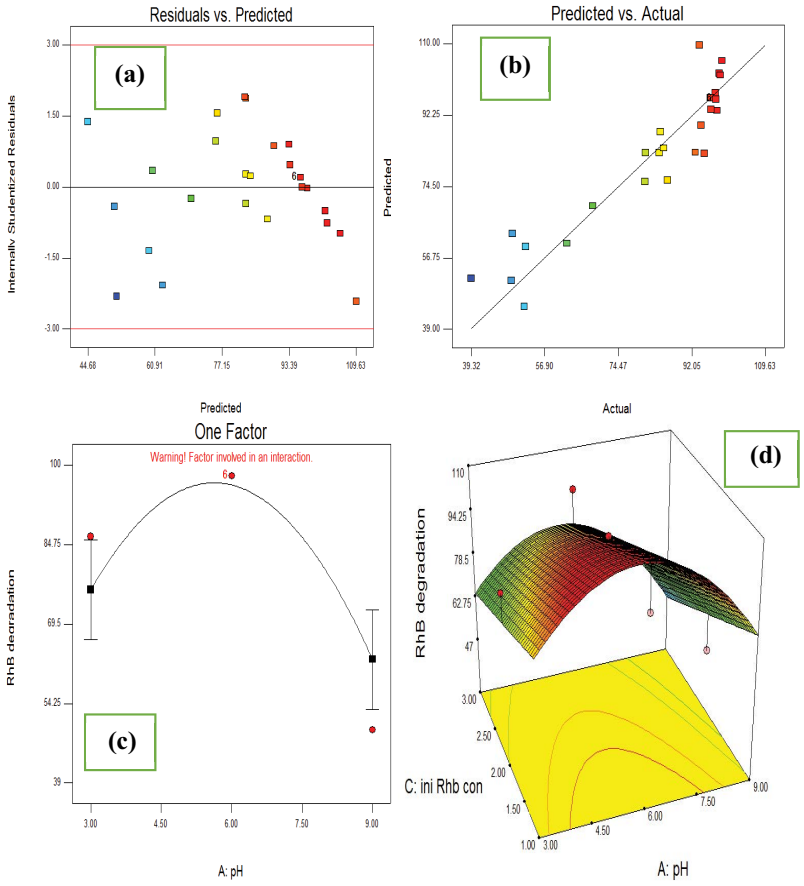


Fig. 6. Plots of (a) residual vs. predicted response for degradation, (b) predicted responses vs. actual experimental values for degradation, (c) one factor and (d) 3D surface for sample S1.

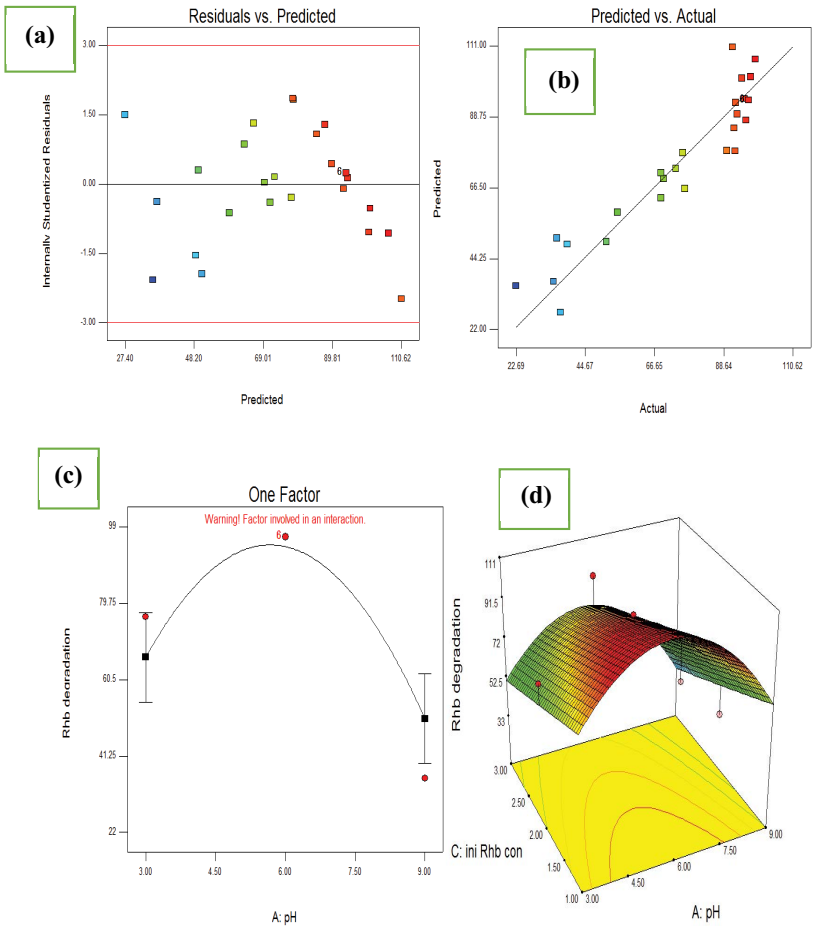


Fig. 7. Plots of (a) residual vs. predicted response for degradation, (b) predicted responses vs. actual experimental values for degradation, (c) one factor and (d) 3D surface for sample H1.

Optimum conditions for experiments were obtained by RSM to maximum degradation of RhB, maximum RhB concentration and minimum catalyst concentration including the; pH = 5.54 and time = 5 h for sample S1, and pH = 5.74 and time = 5 h for sample H1.

## References

[1] A. Payan, M. Fattahi, B. Roozbehani, Synthesis, characterization and evaluations of $TiO_2$ nanostructures prepared from different titania precursors for photocatalytic degradation of 4-chlorophenol in aqueous solution, J. Environ. Health Sci. Eng., 16 (2018) 41–54.

[2] A. Payan, M. Fattahi, S. Jorfi, B. Roozbehani, S. Payan, Synthesis and characterization of titanate nanotube/single-walled carbon nanotube (TNT/SWCNT) porous nanocomposite and its photocatalytic activity on 4-chlorophenol degradation under UV and solar irradiation, Appl. Surf. Sci., 434 (2018) 336–350.

[3] A. Shojaie, M. Fattahi, S. Jorfi, B. Ghasemi, Hydrothermal synthesis of Fe-$TiO_2$-Ag nano-sphere for photocatalytic degradation of 4-chlorophenol (4-CP): investigating the effect of hydrothermal temperature and time as well as calcination temperature, J. Environ. Chem. Eng., 5 (2017) 4564–4572.

[4] B.K. Zhang, Q. Li, D.B. Wang, J.Z. Wang, B.J. Jiang, S.J. Jiao, D.H. Liu, Z. Zeng, C.C. Zhao, Y.X. Liu, Z.K. Xun, X. Fang, S.Y. Gao, Y. Zhang, L.C. Zhao, Efficient photocatalytic hydrogen evolution over $TiO_{2-X}$ mesoporous spheres-ZnO nanorods heterojunction, Nanomaterials (Basel), 10 (2020) 2096, doi: 10.3390/nano10112096.

[5] L. Horváth, Dry deposition velocity of PM2.5 ammonium sulfate particles to a Norway spruce forest on the basis of S- and N-balance estimations, Atmos. Environ., 37 (2003) 4419–4424.

[6] O. Carp, C.L. Huisman, A. Reller, Photoinduced reactivity of titanium dioxide, Prog. Solid State Chem., 32 (2004) 33–177.

[7] H. Kim, K. Jeong, D. Bae, Synthesis and characterization of Fe-doped $TiO_2$ nanoparticles by a sol–gel and hydrothermal process, Korean J. Mater. Res., 22 (2012) 249–252.

[8] Ü. Özgür, Ya.I. Alivov, C. Liu, A. Teke, M.A. Reshchikov, S. Doğan, V. Avrutin, S.-J. Cho, H. Morkoç, A comprehensive review of ZnO materials and devices, J. Appl. Phys., 98 (2005) 041301, doi: 10.1063/1.1992666.

[9] C. Klingshirn, ZnO: material, physics and applications, ChemPhysChem, 8 (2007) 782–803.

[10] P. Nuengmatcha, S. Chanthai, R. Mahachai, W.-C. Oh, Visible light-driven photocatalytic degradation of Rhodamine B and industrial dyes (texbrite BAC-L and texbrite NFW-L) by ZnO-graphene-$TiO_2$ composite, J. Environ. Chem. Eng., 4 (2016) 2170–2177.

[11] N. Farhadian, R. Akbarzadeh, M. Pirsaheb, T.-C. Jen, Y. Fakhri, A. Asadi, Chitosan modified N, S-doped $TiO_2$ and N, S-doped ZnO for visible light photocatalytic degradation of tetracycline, Int. J. Biol. Macromol., 132 (2019) 360–373.

[12] A. Taufik, A. Albert, R. Saleh, Sol–gel synthesis of ternary CuO/$TiO_2$/ZnO nanocomposites for enhanced photocatalytic performance under UV and visible light irradiation, J. Photochem. Photobiol., A, 344 (2017) 149–162.

[13] M.A.M. Adnan, B.L. Phoon, N.M. Julkapli, Mitigation of pollutants by chitosan/metallic oxide photocatalyst: a review, J. Cleaner Prod., 261 (2020) 121190, doi: 10.1016/j.jclepro.2020.121190.
[14] C.C. Pei, W. Woon-Fong Leung, Photocatalytic degradation of Rhodamine B by $TiO_2$/ZnO nanofibers under visible-light irradiation, Sep. Purif. Technol., 114 (2013) 108–116.
[15] J.D. Chen, W.S. Liao, Y. Jiang, D.N. Yu, M.L. Zou, H. Zhu, M. Zhang, M.L. Du, Facile fabrication of ZnO/$TiO_2$ heterogeneous nanofibres and their photocatalytic behaviour and mechanism towards Rhodamine B, Nanomater. Nanotechnol., 6 (2016) 1–9.
[16] R.H. Zha, R. Nadimicherla, X. Guo, Ultraviolet photocatalytic degradation of methyl orange by nanostructured $TiO_2$/ZnO heterojunctions, J. Mater. Chem. A, 3 (2015) 6565–6574.
[17] G.S. Pozan, A. Kambur, Significant enhancement of photocatalytic activity over bifunctional ZnO–$TiO_2$ catalysts for 4-chlorophenol degradation, Chemosphere, 105 (2014) 152–159.
[18] X.M. Xu, J.F. Wang, J. Tian, X. Wang, J. Dai, X. Liu, Hydrothermal and post-heat treatments of $TiO_2$/ZnO composite powder and its photodegradation behavior on methyl orange, Ceram. Int., 37 (2011) 2201–2206.
[19] Z.H. Zhuge, X.J. Liu, T.Q. Chen, Y.Y. Gong, C. Li, L.Y. Niu, S.Q. Xu, X.T. Xu, Z.A. Alothman, C.Q. Sun, J.G. Shapter, Y. Yamauchi, Highly efficient photocatalytic degradation of different hazardous contaminants by $CaIn_2S_4$-$Ti_3C_2T_x$ Schottky heterojunction: an experimental and mechanism study, Chem. Eng. J., 421 (2020) 127838, doi: 10.1016/j.cej.2020.127838.
[20] X.J. Liu, B.B. Liu, L. Li, Z.H. Zhuge, P.B. Chen, C. Li, Y.Y. Gong, L.Y. Niu, J.Y. Liu, L. Lei, C.Q. Sun, $Cu_2In_2ZnS_5$/$Gd_2O_2S$: Tb for full solar spectrum photoreduction of Cr(VI) and $CO_2$ from UV/vis to near-infrared light, Appl. Catal., B, 249 (2019) 82–90.
[21] B.B. Liu, X.J. Liu, J.Y. Liu, C.J. Feng, Z. Li, C. Li, Y.Y. Gong, L.K. Pan, S.Q. Xu, C.Q. Sun, Efficient charge separation between UiO-66 and $ZnIn_2S_4$ flowerlike 3D microspheres for photoelectronchemical properties, Appl. Catal., B, 226 (2018) 234–241.
[22] Z.X. Ren, X.J. Liu, Z.H. Zhuge, Y.Y. Gong, C.Q. Sun, $MoSe_2$/ZnO/ZnSe hybrids for efficient Cr(VI) reduction under visible light irradiation, Chin. J. Catal., 41 (2020) 180–187.
[23] B.B. Liu, X.J. Liu, L. Li, Z.H. Zhuge, Y.Q. Li, C. Li, Y.Y. Gong, L.Y. Niu, S.Q. Xu, C.Q. Sun, $CaIn_2S_4$ decorated $WS_2$ hybrid for efficient Cr(VI) reduction, Appl. Surf. Sci., 484 (2019) 300–306.
[24] R.S. Sabry, Y.K. Al-Haidarie, M.A. Kudhier, Synthesis and photocatalytic activity of $TiO_2$ nanoparticles prepared by sol–gel method, J. Sol-Gel Sci. Technol., 78 (2016) 299–306.
[25] T. Theivasanthi, M. Alagar, Titanium dioxide ($TiO_2$) nanoparticles XRD analyses: an insight, Chem. Phys., 1307 (2013) 1091
[26] G.A. Tompsett, L. Krogh, D.W. Griffin, W.C. Conner, Hysteresis and scanning behavior of mesoporous molecular sieves, Langmuir, 21 (2005) 8214–8225.
[27] R. Beranek, H. Kisch, Tuning the optical and photoelectrochemical properties of surface-modified $TiO_2$, Photochem. Photobiol. Sci., 7 (2008) 40–48.
[28] G. Xiong, U. Pal, J.G. Serrano, K.B. Ucer, R.T. Williams, Photoluminescence and FTIR study of ZnO nanoparticles: the impurity and defect perspective, Phys. Status Solidi A, 3581 (2006) 3577–3581.
[29] H. Kumar, R. Rani, Structural and optical characterization of ZnO nanoparticles synthesized by microemulsion route, Int. Lett. Chem. Phys. Astron., 14 (2013) 26–36.
[30] M.A. Gondal, A.M. Ilyas, T.A. Fasasi, M.A. Dastageer, Z.S. Seddigi, T.F. Qahtan, M. Faiz, G.D. Khattak, Synthesis of green $TiO_2$/ZnO/CdS hybrid nano-catalyst for efficient light harvesting using an elegant pulsed laser ablation in liquids method, Appl. Surf. Sci., 357 (2015) 2217–2222.
[31] Z. Mesgari, M. Gharagozlou, A. Khosravi, K. Gharanjig, Spectrophotometric studies of visible light induced photocatalytic degradation of methyl orange using phthalocyanine-modified Fe-doped $TiO_2$ nanocrystals, Spectrochim. Acta, Part A., 92 (2012) 148–153.
[32] S. Mohammadzadeh, M.E. Olya, A.M. Arabi, A. Shariati, M.R. Khosravi Nikou, Synthesis, characterization and application of ZnO-Ag as a nanophotocatalyst for organic compounds degradation, mechanism and economic study, J. Environ. Sci., 35 (2016) 194–207.
[33] N. Sobana, M. Swaminathan, The effect of operational parameters on the photocatalytic degradation of acid red 18 by ZnO, Sep. Purif. Technol., 56 (2007) 101–107.
[34] L.K. Wang, Y.T. Hung, N.K. Shammas, Advanced Physicochemical Treatment Processes, Humana Press, New Jersey, 2006, pp. 463–481.
[35] A. Hernández Battez, R. González, J.L. Viesca, J.E. Fernández, J.M. Díaz Fernández, A. Machado, R. Chou, J. Riba, CuO, $ZrO_2$ and ZnO nanoparticles as antiwear additive in oil lubricants, Wear, 265 (2008) 422–428.
[36] K. Siwińska-Stefańska, A. Kubiak, A. Piasecki, J. Goscianska, G. Nowaczyk, S. Jurga, T. Jesionowski, $TiO_2$-ZnO binary oxide systems: Comprehensive characterization and tests of photocatalytic activity, Materials (Basel), 11 (2018) 841, doi: 10.3390/ma11050841.